Appl Phys B (2011) 104:343–355
DOI 10.1007/s00340-011-4382-x

Applied Physics B
Lasers and Optics

The effect of particle aggregation on the absorption and emission properties of mono- and polydisperse soot aggregates

F. Liu · G.J. Smallwood

Received: 18 September 2010 / Revised version: 2 December 2010 / Published online: 18 February 2011

Abstract This study concerns the effect of soot-particle aggregation on the soot temperature derived from the signal ratio in two-color laser-induced incandescence measurements. The emissivity of aggregated fractal soot particles was calculated using both the commonly used Rayleigh–Debye–Gans fractal-aggregate theory and the generalized Mie-solution method in conjunction with numerically generated fractal aggregates of specified fractal parameters typical of flame-generated soot. The effect of aggregation on soot temperature was first evaluated for monodisperse aggregates of different sizes and for a lognormally distributed aggregate ensemble at given signal ratios between the two wavelengths. Numerical calculations were also conducted to account for the effect of aggregation on both laser heating and thermal emission at the two wavelengths for determining the effective soot temperature of polydisperse soot aggregates. The results show that the effect of aggregation on laser energy absorption is important at low fluences. The effect of aggregation on soot emissivity is relatively unimportant in LII applications to typical laminar diffusion flames at atmospheric pressure, but it can become more important in flames at high pressures due to larger primary particles and wider aggregate distributions associated with enhanced soot loading.

1 Introduction

Laser-induced incandescence (LII) techniques have become increasingly popular as a preferred approach for measurements of soot in many applications ranging from laminar and turbulent flames, engine combustion, engine exhaust, and black carbon production to flame synthesis of metal oxide particles [1]. The popularity of LII can be primarily attributed to its advantages over conventional methods, such as high spatial and temporal resolution, ease of implementation, and versatility. LII makes use of the light absorption and emission properties of nano-sized absorbing particles by thermally energizing them with the use of a high-energy laser pulse of about 20 ns duration. In such applications, the particle temperature increases rapidly from the ambient temperature to somewhere close to the particle sublimation temperature during the laser pulse and then cools slowly back to the ambient temperature mainly through sublimation and heat conduction. Detection of time-resolved incandescence signals allows the determination of particle concentration and primary particle size information, since the strength of the incandescence signal is proportional to the particle volume fraction [2] and the cooling rate of the particle is related to the particle size [3].

To monitor the extent of soot-particle sublimation, to help gain insights into the nano-scale heat and mass transfer processes during LII, and to provide indispensable data to validate LII models, it is highly desirable to conduct time-resolved LII measurements at multiple detection wavelengths (at least two) in order to obtain the time-resolved soot temperature during the laser heating and the subsequent cooling. In addition to these reasons, the time-resolved soot temperature in LII measurements is also required by the absolute LII intensity method to determine the soot volume fraction [4], for the determination of soot absorption function, $E(m)$, using the low-fluence LII method [5], and for the determination of primary soot-particle diameter distribution [6, 7]. Therefore, two-color LII (2C-LII), in which the incandescence signals are detected at two wavelengths so that

F. Liu (✉) · G.J. Smallwood
Institute for Chemical Process & Environmental Technology, National Research Council, Building M-9, 1200 Montreal Road, Ottawa, Ontario, Canada K1A 0R6
e-mail: Fengshan.liu@nrc-cnrc.gc.ca

soot temperature can be inferred from the signal ratio with the help of a model describing the soot-particle emissivity at the two detection wavelengths, has become the preferred way to conduct LII experiments [1].

Although LII has been demonstrated to be applicable to non-soot nanoparticles, e.g. [1], it has been primarily used for measurements of combustion-generated soot. Since the optical properties of particles are dependent on their shape and size, it is important to know the morphology of soot particles in order to accurately predict their absorption and emission properties, which are essential in the context of LII theory and practice. It has been well established that combustion-generated soot forms mass alike fractal aggregates consisting of nearly spherical primary particles [8, 9], as a result of particle aggregation. The aggregate size (the number of primary particles) has been found to cover a wide distribution from 1 (isolated primary particles) to several hundreds (in laminar diffusion flames) or even thousands (in turbulent flames). The primary particle diameter, however, has a relatively narrow distribution from 10 to 60 nm. Within a given soot aggregate the primary particles can be considered approximately uniform in size. It has been shown in a vast body of literature that the fractal dimension of combustion-generated soot falls in a narrow range of 1.6 to 1.9, which implies that the fractal structure of soot is fairly open. As a consequence of particle aggregation, the mass alike fractal soot aggregates have different thermal and optical properties from those of isolated primary particles. To better quantitatively model the heat and mass transfer processes during laser heating and subsequent cooling in LII it is important to account for the various effects of particle aggregation. In particular, the effects of aggregation on the laser energy absorption, heat conduction, sublimation, and thermal emission are of importance within the context of LII modelling. The effect of aggregation on heat conduction has been investigated by Filippov et al. [10] and more recently by Liu et al. [11], Liu and Smallwood [12], and Daun [13]. However, these studies were conducted almost exclusively in the free-molecular regime with only one effort in the transition regime [12], which is relevant to LII experiments conducted at elevated pressures. The effect of aggregation on laser energy absorption in LII modelling has been recently investigated by Liu and Smallwood [14] for monodisperse aggregates. To our knowledge, there have been no studies to address the effect of aggregation on sublimation. The present study concerns the effect of polydisperse aggregation on the absorption properties, and mono- and polydisperse aggregation on the emission properties of soot aggregates, with emphasis on the latter.

The complex and rather open structure of fractal soot aggregates implies that their optical properties cannot be described by the Mie theory applied to a spherical equivalent of the aggregate [15, 16]. Although it has been shown in several studies that the Rayleigh–Debye–Gans fractal-aggregate (RDG-FA) theory provides a fairly accurate description of the optical properties of soot, e.g., [17], provided that the refractive index of soot is known, the RDG-FA theory unfortunately cannot account for the effect of aggregation on absorption and predicts that the aggregate absorption cross section is simply the summation of all the individual primary particle absorption cross sections. Numerical calculations using more accurate theoretical models have shown that the RDG-FA theory in general underestimates the aggregate cross section by about 10%, depending on the aggregate size and primary particle size parameter [14]. It has been pointed out by Liu et al. [14, 18] that an error of this magnitude in the soot absorption cross section is not acceptable in LII modelling, especially in the low-fluence regime where soot sublimation is negligible. Our recent study has cast doubts on the adequacy of the RDG-FA theory to LII modelling [14], since this approximate theory completely neglects the effect of aggregation on the absorption and emission properties of fractal aggregates.

In the determination of soot temperature in 2C-LII from the ratio of the detected LII intensities at two wavelengths, the ratio of soot-particle emissivities at the detection wavelengths is required. So far the RDG-FA theory has been used in practice with 2C-LII to arrive at the soot temperature. Based on the recent progress in the quantitative understanding of the effect of aggregation on the aggregate absorption cross section, it is anticipated that aggregation has the same effect on the emissivity of soot aggregates and could potentially affect the soot temperature derived from the incandescence signal ratio in 2C-LII measurements. However, the effect of aggregation on the soot temperature determined in 2C-LII measurements has not been investigated. Motivated by this observation, a numerical study was conducted to understand quantitatively (i) how aggregation affects the soot temperature based on given incandescence signal ratios for both monodisperse and polydisperse aggregates, and (ii) how aggregation affects the effective soot temperature of a polydisperse ensemble of aggregates based on the predicted incandescence signal ratio that takes into account the aggregation effect on the laser energy absorption rate.

2 Theory

2.1 Relationship between soot temperature and LII signal ratio

The blackbody radiant emission intensities of a (macroscopic) surface of temperature T at two different wavelengths λ_1 and λ_2 are given as

$$I_{b\lambda_1} = \frac{C_1}{\lambda_1^5} \frac{1}{\exp(C_2/\lambda_1 T) - 1}, \tag{1}$$

$$I_{b\lambda_2} = \frac{C_1}{\lambda_2^5}\frac{1}{\exp(C_2/\lambda_2 T)-1}, \tag{2}$$

where $I_{b\lambda}$ is the power radiated per steradian per unit surface area and per unit wavelength interval (radiation intensity) for a blackbody, $C_1 = 2hc^2$, $C_2 = hc/k$, h is the Planck constant, c is the speed of light, and k is the Boltzmann constant. Without losing generality, it is assumed throughout this work that $\lambda_2 > \lambda_1$. In this study, as in almost all previous studies, it is assumed that soot aggregates consist of identical primary spherical particles of diameter d_p that are in point touch. Although these assumptions are reasonable based on image analysis of soot sampled from various flames, it should be recognized that there are small variations in size among primary particles within an aggregate and there is certain degree of overlap and/or necking/bridging between connecting primary particles, i.e., primary particles are not in point touch. The primary soot particles are in general in the range of 10 to 60 nm and are sufficiently small to be considered in the Rayleigh regime for wavelengths in the visible spectral range. In the following analysis, the size of an aggregate is represented by the number of primary spherical particles it contains. For an arbitrarily shaped particle its emissivity is equal to its absorption efficiency [19]. Applying this principle to an aggregate at a wavelength λ leads to

$$Q_{abs}^{agg} = \varepsilon_p^{agg}, \tag{3}$$

where the superscript agg represents quantities of aggregate, Q_{abs} is the particle absorption efficiency and ε_p is the particle emissivity. For an aggregate of size N_p its absorption efficiency is written as

$$Q_{abs}^{agg} = \frac{C_{abs}^{agg}}{N_p A_{geo}^{p}}, \tag{4}$$

i.e., it is the ratio of the aggregate absorption cross section C_{abs}^{agg} to the total cross sectional area of all the constituent primary particles, where A_{geo}^{p} is the geometric cross sectional area of a primary particle. It should be noted that in the following analysis, the superscript p indicates primary particle quantities.

For an aggregate consisting of N_p primary particles at temperature T its emitted powers q_λ at λ_1 and λ_2 are

$$\begin{aligned} q_{\lambda_1} &= N_p \pi d_p^2 I_{b\lambda_1} \varepsilon_{p_1}^{agg} \\ &= N_p \pi d_p^2 \varepsilon_{p_1}^{agg} \frac{C_1}{\lambda_1^5}\frac{1}{\exp(C_2/\lambda_1 T)-1}, \end{aligned} \tag{5}$$

$$\begin{aligned} q_{\lambda_2} &= N_p \pi d_p^2 I_{b\lambda_2} \varepsilon_{p_2}^{agg} \\ &= N_p \pi d_p^2 \varepsilon_{p_2}^{agg} \frac{C_1}{\lambda_2^5}\frac{1}{\exp(C_2/\lambda_2 T)-1}. \end{aligned} \tag{6}$$

The detected LII signals S_λ at λ_1 and λ_2 can be related to the particle emission intensities, the detection bandwidths, the soot volume fraction (or soot number density), the detection volume, the transmission characteristics of the filters, and the spectral responses of the detectors. Assuming the optical path-length of the incandescent particles along the detection direction is small so that the optically thin approximation is valid and the bandwidths of the two detection wavelengths are sufficiently narrow, the detected LII signal current can be written as

$$\begin{aligned} S_{\lambda_1} &= C\int_{\lambda_1-\delta\lambda_1/2}^{\lambda_1+\delta\lambda_1/2} q_{\lambda_1}\tau_{\lambda_1} D_{\lambda_1}\, d\lambda \\ &\approx C\frac{N_p \pi d_p^2 \varepsilon_{p_1}^{agg}\delta\lambda_1\tau_1 D_1}{\lambda_1^5}\frac{C_1}{\exp(C_2/\lambda_1 T)-1}, \end{aligned} \tag{7}$$

$$\begin{aligned} S_{\lambda_2} &= C\int_{\lambda_2-\delta\lambda_2/2}^{\lambda_2+\delta\lambda_2/2} q_{\lambda_2}\tau_{\lambda_2} D_{\lambda_2}\, d\lambda \\ &\approx C\frac{N_p \pi d_p^2 \varepsilon_{m_2}^{agg}\delta\lambda_2\tau_2 D_2}{\lambda_2^5}\frac{C_1}{\exp(C_2/\lambda_2 T)-1}, \end{aligned} \tag{8}$$

where $\delta\lambda_1$ and $\delta\lambda_2$ are the respective bandwidths at center wavelength λ_1 and λ_2 and constant C accounts for all factors other than bandwidth $\delta\lambda$, filter transmissivity τ, and the detector response D. The signal ratio R can then be written as

$$R = \frac{S_{\lambda_1}}{S_{\lambda_2}} = \frac{\delta\lambda_1}{\delta\lambda_2}\frac{\tau_1 D_1 \varepsilon_{m_1}^{agg}}{\tau_2 D_2 \varepsilon_{m_2}^{agg}}\frac{\lambda_2^5}{\lambda_1^5}\frac{\exp(C_2/\lambda_2 T)-1}{\exp(C_2/\lambda_1 T)-1}. \tag{9}$$

Using a revised signal ratio $\Re = R\delta\lambda_2\tau_2 D_2/\delta\lambda_1\tau_1 D_1$, (9) can be rewritten as

$$\Re = \frac{s_1}{s_2} = \phi\frac{\lambda_2^5}{\lambda_1^5}\frac{\exp(C_2/\lambda_2 T)-1}{\exp(C_2/\lambda_1 T)-1}, \tag{10}$$

where

$$\phi = \frac{\varepsilon_{p_1}^{agg}}{\varepsilon_{p_2}^{agg}} \tag{11}$$

is the soot aggregate emissivity ratio and s_1 and s_2 are the revised signals, i.e., $s_1 = S_{\lambda_1}/\delta\lambda_1\tau_1 D_1$, $s_2 = S_{\lambda_2}/\delta\lambda_2\tau_2 D_2$. The purposes of introducing the revised signals s_1 and s_2 (and the revised signal ratio $\Re$) are to simplify the equations developed below and highlight the relationships among the soot temperature T, the signal ratio $\Re$, and the soot aggregate emissivity ratio ϕ. It is important to note that for a given pair of detection wavelengths the revised signals s_1 and s_2 are proportional to the unrevised signals S_{λ_1} and S_{λ_2}, albeit the proportional constants are in general different. The detected LII signal S can be conveniently scaled to obtain the revised signal s according to the definitions above. For these reasons, only the revised signals s_1 and s_2 and their ratio

$\Re$ are considered in the following analysis. It should also be noted that the word *revised* is dropped in what follows for simplicity. For a known signal ratio $\Re$, the soot-particle temperature T can be calculated approximately, using Wien approximation and (10), as

$$T = -C_2\left(\frac{1}{\lambda_1} - \frac{1}{\lambda_2}\right)\frac{1}{\ln(\Re\frac{1}{\phi}\frac{\lambda_1^5}{\lambda_2^5})}. \tag{12}$$

Using this approximate temperature as the first guess, a very accurate soot temperature can be obtained using the iterative method suggested by Levendis et al. [20].

The formulations presented above are applicable only to monodisperse aggregates. For polydisperse aggregates, it is necessary to know the aggregate size distribution. When the polydispersity of aggregate size is considered, however, it is assumed that the primary particle diameters are still uniform for different sized aggregates in this study, though it is possible to allow variation of the primary particle diameter from aggregate to aggregate [11]. For combustion-generated soot the aggregate size distribution can be conveniently and reasonably described by a lognormal distribution given as

$$p(N_\mathrm{p}) = \frac{1}{N_\mathrm{p}\sqrt{2\pi}\ln\sigma_\mathrm{g}}\exp\left[-\left(\frac{\ln(N_\mathrm{p}/N_\mathrm{g})}{\sqrt{2}\ln\sigma_\mathrm{g}}\right)^2\right], \tag{13}$$

where N_g and σ_g are the two parameters of the distribution function and represent respectively the geometric mean aggregate size and the geometric standard deviation. For polydisperse soot aggregates although the temperatures of different sized aggregates are in general different during the laser heating [14] and subsequent cooling [11], all the aggregates can still be considered at an effective temperature T_e as far as radiant power is concerned, which is also the so-called pyrometric temperature and is determined from the ratio of radiation intensities at two different wavelengths. For a lognormally distributed ensemble of aggregates at an effective temperature T_e its emitted powers at λ_1 and λ_2 are

$$\begin{aligned} q_{\lambda_1} &= \int_1^\infty N_\mathrm{p}\pi d_\mathrm{p}^2 I_{\mathrm{b}\lambda_1}\varepsilon_{\mathrm{p}1}^{\mathrm{agg}} p(N_\mathrm{p})\,dN_\mathrm{p} \\ &= \frac{C_1}{\lambda_1^5}\frac{\pi d_\mathrm{p}^2}{\exp(C_2/\lambda_1 T_\mathrm{e})-1}\int_1^\infty N_\mathrm{p}\varepsilon_{\mathrm{p}1}^{\mathrm{agg}} p(N_\mathrm{p})\,dN_\mathrm{p}, \end{aligned} \tag{14}$$

$$\begin{aligned} q_{\lambda_2} &= \int_1^\infty N_\mathrm{p}\pi d_\mathrm{p}^2 I_{\mathrm{b}\lambda_2}\varepsilon_{\mathrm{p}2}^{\mathrm{agg}} p(N_\mathrm{p})\,dN_\mathrm{p} \\ &= \frac{C_1}{\lambda_2^5}\frac{\pi d_\mathrm{p}^2}{\exp(C_2/\lambda_2 T_\mathrm{e})-1}\int_1^\infty N_\mathrm{p}\varepsilon_{\mathrm{p}2}^{\mathrm{agg}} p(N_\mathrm{p})\,dN_\mathrm{p}. \end{aligned} \tag{15}$$

Therefore, by replacing the product $N_\mathrm{p}\varepsilon_\mathrm{p}^{\mathrm{agg}}$ with $\int_1^\infty N_\mathrm{p}\varepsilon_\mathrm{p}^{\mathrm{agg}} p(N_\mathrm{p})\,dN_\mathrm{p}$, a similar derivation to that used for monodisperse aggregates to arrive at (10) can still be followed for polydisperse aggregates. The relationship between the effective temperature and the signal ratio for polydisperse aggregates can be written as

$$\Re = \phi^{\mathrm{poly}}\frac{\lambda_2^5}{\lambda_1^5}\frac{\exp(C_2/\lambda_2 T_\mathrm{e})-1}{\exp(C_2/\lambda_1 T_\mathrm{e})-1}, \tag{16}$$

where

$$\phi^{\mathrm{poly}} = \frac{\int_1^\infty N_\mathrm{p}\varepsilon_{\mathrm{p}1}^{\mathrm{agg}} p(N_\mathrm{p})\,dN_\mathrm{p}}{\int_1^\infty N_\mathrm{p}\varepsilon_{\mathrm{p}2}^{\mathrm{agg}} p(N_\mathrm{p})\,dN_\mathrm{p}} \tag{17}$$

is the ratio of polydisperse aggregate emissivity at wavelengths λ_1 to that at λ_2.

2.2 Absorption cross section of soot aggregates

Equations (10) and (16) indicate that it is essential to know the soot aggregate emissivity ratio at the two detection wavelengths to determine the effective soot temperature for a known signal ratio $\Re$, which is obtained in 2C-LII measurements. To arrive at the soot aggregate emissivity ratio the absorption cross sections of soot aggregates at the two detection wavelengths must be known. Although the structure of combustion-generated soot appears complex, it can be conveniently described by the following statistical scaling relationship

$$N_\mathrm{p} = k_\mathrm{f}\left(\frac{R_\mathrm{g}}{a}\right)^{D_\mathrm{f}}, \tag{18}$$

where N_p is the number of primary particles (aggregate size), R_g is the radius of gyration, a is the radius of primary particle, and k_f and D_f are the fractal prefactor and fractal dimension, respectively. In this study, two aggregate absorption models are used to calculate the absorption cross section of soot aggregates. The first model considered is the RDG-FA theory, which has been commonly adopted in LII studies, and the second one is a numerically exact approach for multi-sphere clusters, described later.

In the RDG-FA approximation, the effect of aggregation on aggregate absorption is completely neglected and the aggregate cross section is simply the summation of the cross sections of all the primary particles, i.e.,

$$C_\mathrm{abs}^{\mathrm{agg}} = N_\mathrm{p}C_\mathrm{abs}^{\mathrm{p}}, \tag{19}$$

where the absorption cross section of primary particles is that in the Rayleigh regime

$$C_\mathrm{abs}^{\mathrm{p}} = \frac{\pi^2 d_\mathrm{p}^3 E_m}{\lambda}, \tag{20}$$

and E_m is the absorption function of the complex refractive index m given as

$$E_m = \mathrm{Im}\left(\frac{m^2-1}{m^2+2}\right). \tag{21}$$

The validity of (19) requires the particle size parameter $x_p = \pi d_p/\lambda$ to be in the Rayleigh regime, such that x_p is less than approximately 0.3 [21]. The consequence of using the RDG-FA theory is that the aggregate emissivity is the same as that of the primary particle. As a result, with RDG-FA theory the emissivity ratios for both monodisperse and polydisperse aggregates are the same and given as

$$\phi = \phi^{\text{poly}} = \frac{E_{m1}}{E_{m2}} \frac{\lambda_2}{\lambda_1}. \tag{22}$$

More accurate theoretical models than the RDG-FA theory have been developed over the last few decades to predict the optical properties of fractal aggregates, such as the volume integral equation formulation (VIEF) [22], coupled electric and magnetic dipole (CEMD) method [23], discrete-dipole approximation (DDA) [24], the superposition T-Matrix method [25], and the generalized Mie-solution method (GMM) [26, 27]. In these models the positions of individual primary particles are required to carry out the numerical calculations and orientation averaging is necessary to simulate the properties of a random-oriented ensemble of aggregates. The second aggregate absorption model considered in this study is GMM for the reason that it is the numerically exact method to predict the optical properties of non-overlapping multi-sphere systems. It is important to note that GMM is not applicable to overlapping spheres. Therefore, the assumption of point touch primary particles is essential, though not entirely realistic, for employing GMM in the present study and represents the first limitation of this study. To more realistically represent flame-generated soot it is important to account for the overlap between connecting primary particles. Other numerical methods, such as DDA, would be required for this purpose. Nevertheless, investigation of the overlap effect between connecting primary particles is beyond the scope of this work and will be pursued in future studies.

Fractal aggregates consisting of identical and just touching primary spherical particles were first generated numerically using tunable cluster-particle and cluster-cluster aggregation algorithms described in [10, 28] for aggregate size N_p in the range of 5 to 893 with specified morphological parameters typical of combustion-generated soot, i.e., $a = 15$ nm, $k_f = 2.3$, and $D_f = 1.78$. In addition, calculations for a single primary particle ($N_p = 1$) at different size parameters ($x_p = \pi d_p/\lambda$) were also conducted. For a single primary particle, the GMM calculation is identical to Mie theory. Throughout this work the refractive index of soot was assumed to be independent of wavelength and we take the value of $m = 1.6 + 0.6i$, which is again a typical value for soot in the visible spectrum. The corresponding value of E_m is 0.27, which is used in all the numerical calculations whenever the RDG-FA was used. GMM calculations were conducted for several primary particle size parameters

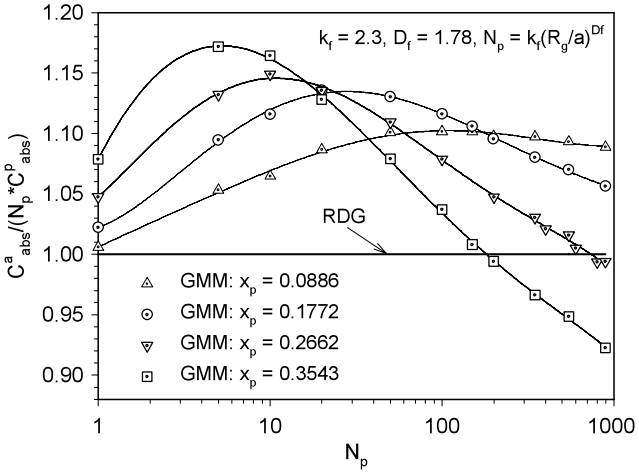

Fig. 1 Variation of the normalized aggregate absorption cross section with aggregate size N_p for different primary particle size parameters. The results were calculated assuming $m = 1.6 + 0.6i$. The lines are 5th order polynomial fit to the numerical results

from $x_p = 0.0886$ up to $x_p = 0.3543$ with at least 3375 orientations to achieve accurate orientation averaged results. In addition, most of the calculations were also carried out for 10 different aggregate realizations of identical morphological parameters (N_p, a, k_f, and D_f) to minimize the effect of realization on the optical properties of these numerically generated aggregates [29].

Results of the normalized aggregate cross sections as a function of the aggregate size for four primary particle size parameters are compared in Fig. 1. Since the RDG-FA theory neglects the effect of particle aggregation and assumes that the primary particles are in the Rayleigh regime, the normalized aggregate absorption cross section remains unity independent of the primary particle size parameter and the aggregate size. The GMM results, however, indicate that the aggregate cross section varies rather significantly with both the primary particle size parameter and the aggregate size. The variation of the aggregate absorption cross section with the aggregate size becomes more pronounced as the primary particle size parameter increases, i.e., it rises more rapidly to a higher value and then decreases faster. These results can be explained by the enhanced importance of particle interference and the shielding effect [23]. It should be noted that the GMM results deviate increasingly from unity for single primary particles ($N_p = 1$) as the primary particle size parameter increases. This is because GMM yields the full Mie solution for $N_p = 1$, rather than the Rayleigh solution valid only for small x_p. To implement the GMM results of the aggregate absorption cross section in the numerical calculations the normalized results shown in Fig. 1 are fit to a 5th order polynomial of the aggregate size. The coefficients of these 5th order polynomials are then further fit to a 3rd order polynomial of the primary particle size parameter.

2.3 LII model

To fully understand the effect of aggregation on laser energy absorption, subsequent cooling and incandescence emission, it is of interest to investigate how aggregation affects the ratio of the incandescence signals and the effective temperature of a lognormally distributed fractal soot aggregate ensemble. In this regard, this study is an extension of our recent work [14], where the effect of aggregation on aggregate thermal emission and the polydispersity of soot aggregates were not considered.

The following aggregate based LII model was used for the purposes of the present study, which is essentially the same model as that used in our recent study [14]. It is formulated in terms of energy and mass conservation written for an aggregate consisting of N_p primary particles

$$\frac{1}{6}\pi d_\mathrm{p}^3 N_\mathrm{p}\rho_\mathrm{s}c_\mathrm{s}\frac{dT}{dt} = C_\mathrm{abs}^\mathrm{agg}F_0 q(t) - q_\mathrm{c} - q_\mathrm{r} + \frac{\Delta H_\mathrm{v}}{M_\mathrm{v}}\frac{dM}{dt}, \tag{23}$$

$$\frac{dM}{dt} = \frac{1}{2}N_\mathrm{p}\rho_\mathrm{s}\pi d_\mathrm{p}^2\frac{dd_\mathrm{p}}{dt} = -\pi d_\mathrm{p}^2 N_\mathrm{p}\beta p_\mathrm{v}\sqrt{\frac{M_\mathrm{v}}{2\pi R_\mathrm{u}T}}, \tag{24}$$

where ρ_s and c_s are the density and specific heat of soot, t is time, F_0 is the laser fluence, $q(t)$ is the laser power temporal profile per unit laser fluence, q_c and q_r are aggregate heat loss rates due to conduction and radiation, respectively. The last term in (23) represents aggregate sublimation heat loss rate with M being the aggregate total mass, M_v the mean molecular weight of the sublimated species, and ΔH_v the heat of sublimation. In (24) p_v is the vapor pressure of the sublimated species, R_u is the universal gas constant, and the effective sublimation coefficient β was chosen as 0.9. Soot aggregate heat loss during and after the laser pulse due to radiation, q_r, and conduction, q_c, were calculated using the expressions given in [11]. Note that the effect of aggregation on heat conduction was taken into account as described in [11]. It is implicitly assumed in (23) and (24) that any potential temperature non-uniformity among primary particles within an aggregate was neglected. It is also worth noting that the effect of aggregation on soot sublimation, the last term on the right hand side of (23), was completely neglected due to a lack of better knowledge, which represents the second limitation of the present study.

The solutions to (23) and (24) are calculated for monodisperse aggregates and monodisperse primary particles of specified N_p and d_p. Because the focus of this study is the effect of aggregation on soot aggregate absorption and emission in LII measurements and modelling, only the polydispersity in aggregate size is taken into account, though it is straightforward to account for polydispersity in both aggregate size and primary particle diameter following our previous study [11]. For a set of prescribed aggregate sizes ranging from 1 to 800, (23) and (24) are first solved to provide time-resolved soot-particle temperature and primary particle diameter for a given initial primary particle diameter and laser fluence. To simulate the effective soot temperature derived in 2C-LII, the total incandescence intensities from a unit volume of laser excited soot/gas mixture containing lognormally distributed aggregates at the two detection wavelengths are first calculated as

$$\begin{aligned} I_{\lambda_1} &= n^\mathrm{agg}\int_1^\infty N_\mathrm{p}\pi d_\mathrm{p}^2 I_{\mathrm{b}\lambda_1}\varepsilon_{\mathrm{p}_1}^\mathrm{agg}p(N_\mathrm{p})\,dN_\mathrm{p} \\ &= \frac{n^\mathrm{agg}C_1}{\lambda_1^5}\int_1^\infty N_\mathrm{p}\varepsilon_{\mathrm{p}_1}^\mathrm{agg}\frac{\pi d_\mathrm{p}^2 p(N_\mathrm{p})}{\exp(C_2/\lambda_1 T)-1}\,dN_\mathrm{p}, \end{aligned} \tag{25}$$

$$\begin{aligned} I_{\lambda_2} &= n^\mathrm{agg}\int_1^\infty N_\mathrm{p}\pi d_\mathrm{p}^2 I_{\mathrm{b}\lambda_2}\varepsilon_{\mathrm{p}_2}^\mathrm{agg}p(N_\mathrm{p})\,dN_\mathrm{p} \\ &= \frac{n^\mathrm{agg}C_1}{\lambda_2^5}\int_1^\infty N_\mathrm{p}\varepsilon_{\mathrm{p}_2}^\mathrm{agg}\frac{\pi d_\mathrm{p}^2 p(N_\mathrm{p})}{\exp(C_2/\lambda_2 T)-1}\,dN_\mathrm{p}, \end{aligned} \tag{26}$$

where n^agg is the aggregate number density. It is important to remember that the soot temperature in the exponential terms in (25) and (26) is calculated from the LII model equations, (23) and (24), and is a function of time and is dependent on the laser fluence, the primary particle diameter, and the aggregate size. Then the ratio of the incandescence intensities at the two wavelengths is used to define the effective soot temperature. This procedure follows that presented earlier leading to (16) and (17); however, in this case the signal ratio $\Re$ is the ratio of the calculated incandescence intensity, i.e., $I_{\lambda_1}/I_{\lambda_2}$, and is given as

$$\Re = \frac{\lambda_2^5}{\lambda_1^5}\frac{\int_1^\infty N_\mathrm{p}\varepsilon_{\mathrm{p}_1}^\mathrm{agg}\frac{\pi d_\mathrm{p}^2}{\exp(C_2/\lambda_1 T)-1}p(N_\mathrm{p})\,dN_\mathrm{p}}{\int_1^\infty N_\mathrm{p}\varepsilon_{\mathrm{p}_2}^\mathrm{agg}\frac{\pi d_\mathrm{p}^2}{\exp(C_2/\lambda_2 T)-1}p(N_\mathrm{p})\,dN_\mathrm{p}}. \tag{27}$$

Once the LII signal ratio is calculated from (27), the effective soot temperature is obtained from (16).

3 Results and discussion

3.1 Effect of aggregation on soot temperature in 2C-LII measurements

The effect of aggregation on soot temperature determined from a known incandescence signal ratio was first investigated for monodisperse aggregates using (10), (11) and the two aggregate absorption models (RDG-FA or RDG for short and GMM). Results for $d_\mathrm{p} = 30$ nm and detection wavelengths of $\lambda_1 = 400$ nm and $\lambda_2 = 780$ nm are compared in Fig. 2 for four aggregate sizes between $N_\mathrm{p} = 10$ and 800 and for a temperature range of 2000 to 4500 K, which covers almost the entire range of soot temperatures encountered in LII measurements. The selection of these two detection wavelengths, i.e., $\lambda_1 = 400$ nm and $\lambda_2 = 780$ nm,

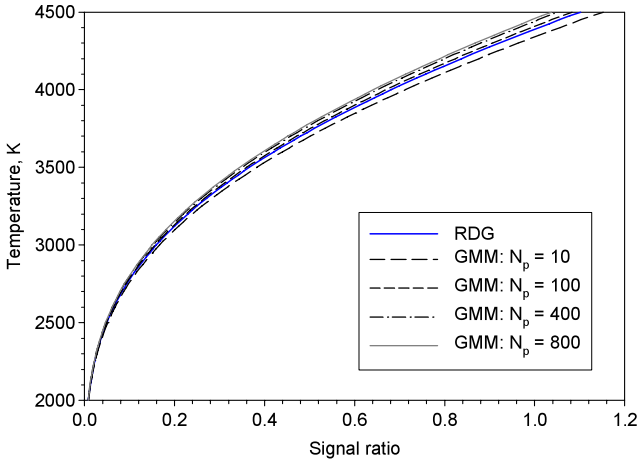

Fig. 2 The relationship of soot temperature vs. signal ratio for monodisperse aggregates of different sizes and $d_p = 30$ nm

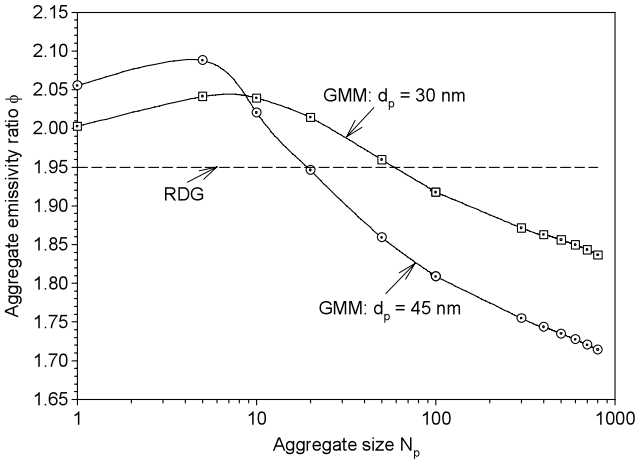

Fig. 3 Variation of the aggregate emissivity ratio with aggregate size

in this study to investigate the effect of particle aggregation on soot emission was based on our recent work [30]. If another pair of detection wavelengths is used in 2C-LII, it is expected that the results presented in this study will be slightly altered quantitatively, but not qualitatively, and will not affect the interpretation of the results. As expected, use of the RDG-FA theory results in a single curve for the temperature vs. two wavelength signal ratio relationship, since the aggregate absorption cross section is independent of the aggregate size as shown in Fig. 1. Use of the GMM model, however, results in aggregate size dependent relationships of temperature vs. signal ratio, which is also expected from the aggregate size dependent aggregate absorption cross section shown in Fig. 1. It can be seen in Fig. 2 that the effect of aggregation on the T vs. $\Re$ relationship is fairly significant and becomes more pronounced as the temperature increases. For example, at a signal ratio of $\Re = 1.0$, the difference in the temperature between $N_p = 10$ and $N_p = 800$ is about 110 K and the neglect of the aggregation effect, i.e., the difference in temperature between the RDG-FA and the GMM at $N_p = 800$, could lead to soot temperature discrepancy by about 80 K. It is interesting to notice that when the aggregation effect is accounted for, the resultant soot temperature can be either lower or higher than that from the RDG-FA theory, depending on the aggregate size. For the conditions assumed in these calculations, the soot temperatures from the GMM model are lower than those from the RDG-FA theory only for $N_p = 10$. This is because at $N_p = 10$ the aggregate emissivity ratio ϕ from the GMM model is higher than that from the RDG-FA theory, but lower than that from RDG-FA theory for the larger aggregates considered, Fig. 3. This effect of ϕ on soot temperature can be easily predicted by (12).

The relationships between the temperature and the two wavelength signal ratio for a primary particle size $d_p =$ 45 nm, detection wavelengths of $\lambda_1 = 400$ nm and $\lambda_2 =$

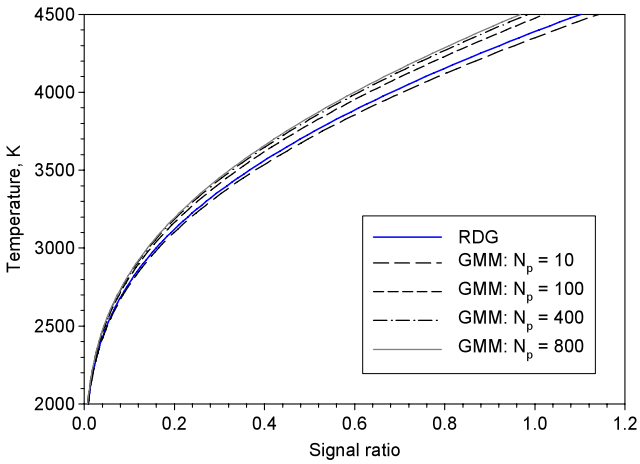

Fig. 4 The relationship of soot temperature vs. signal ratio for monodisperse aggregates of different sizes and $d_p = 45$ nm

780 nm, and different aggregate sizes are shown in Fig. 4. The effect of aggregation is significantly stronger when the primary particle diameter is increased from 30 nm to 45 nm, i.e., at a given signal ratio the deviations of temperature based on the GMM model from that based on the RDG-FA become much larger, compare Figs. 2 and 4. It should be noted that a larger primary particle diameter means a larger primary particle size parameter at the two considered detection wavelengths. Consequently, the aggregate emissivity displays a larger variation with the aggregate size as revealed by the aggregate absorption cross sections shown in Fig. 1. As a result of the stronger variation of the aggregate emissivity with aggregate size at larger primary particle size parameters, the ratio of the aggregate emissivities at the two detection wavelengths has a larger deviation from the RDG-FA value. A larger deviation in the emissivity ratio from the RDG value is the reason why the aggregation effect becomes more significant when d_p is increased from 30 to 45 nm. This is clearly illustrated in Fig. 3, where the GMM curve

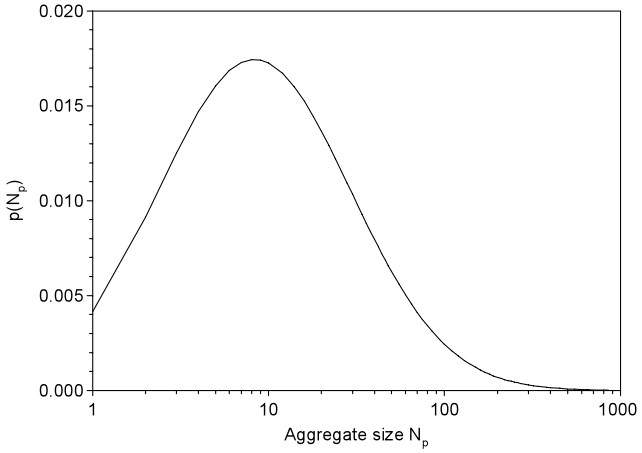

Fig. 5 Lognormal distribution for $N_g = 40$ and $\sigma_g = 3.5$

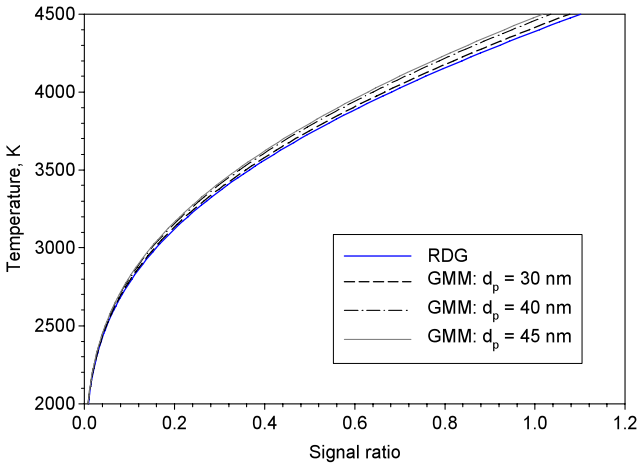

Fig. 6 The relationship between the signal ratio and the effective soot temperature for polydisperse aggregates and three different primary particle diameters

for $d_p = 45$ nm displays a greater variation with the aggregate size and a larger deviation from the RDG-FA value than that for $d_p = 30$ nm.

Although the results shown in Figs. 2 and 4 are useful for interpreting the effect of aggregation on the relationship between soot temperature and the signal ratio for monodisperse aggregates, it is also important to evaluate the effect of aggregation on this relationship for lognormally distributed aggregates, since combustion-generated soot in general consists of polydisperse aggregates that follow a distribution closely approximated by a lognormal. Limited by the maximum aggregate size N_p of 893 in the present results for the GMM aggregate absorption model shown in Fig. 1, a lognormal distribution of N_p with $N_g = 40$ and $\sigma_g = 3.5$ was used to represent a typical polydisperse distribution of soot aggregates in laminar diffusion flames [31]. This lognormal distribution is shown in Fig. 5. The distribution probability function drops to almost 1.0×10^{-5} at $N_p = 900$ so that the contribution from larger aggregates to the integrations associated with the distribution function, e.g., (17), can be neglected. The effect of aggregation on the relationship between the effective temperature and the signal ratio, again at detection wavelengths of $\lambda_1 = 400$ nm and $\lambda_2 = 780$ nm used throughout this study, for a lognormally distributed ensemble of aggregates and three different primary particle diameters is shown in Fig. 6. The fairly small deviation of the GMM curve for $d_p = 30$ nm from the RDG one suggests that the effect of aggregation on the relationship between the temperature and the signal ratio can be neglected in 2C-LII experiments conducted in laminar diffusion flames at atmospheric pressure, since $d_p = 30$ nm and the lognormal distribution function used in these calculations represent typical primary particle diameter and aggregate size distribution in such flames. It is well known that soot concentrations increase rapidly with pressure [32] and it is very plausible that the primary particle diameters are much bigger and the aggregate size distributions are much wider for soot generated in high pressure flames. Results shown in Fig. 6 indicate that the deviation of the GMM curve from the RDG one increases fairly quickly with increasing the primary particle diameter while keeping the aggregate size distribution unchanged. At $d_p = 45$ nm, neglect of the aggregation effect on soot-particle emissivity could lead to an error in the temperature by as much as about 100 K at high temperatures. Therefore, it is reasonable to conclude that the effect of aggregation on soot aggregate emission can be neglected in 2C-LII experiments in laminar diffusion flames at atmospheric pressure; however, such effect should be accounted for in diffusion flames at high pressures. Based on the principle of the absolute LII intensity approach [4], with LII signals detected at 400 and 780 nm, a 10% error in the emissivity ratio due entirely to an error in the soot emissivity at $\lambda_1 = 400$ nm would give rise to a relative error about 20% in the derived soot volume fraction. If the assumed 10% error in the emissivity ratio is caused by error in the soot emissivity at $\lambda_2 = 780$ nm, the resultant relative error in the derived soot volume fraction would be about 10%. It is noted that the relative error in the derived soot volume fraction is dependent only on the detection wavelengths and the relative error in the soot aggregate emissivities at the two detection wavelengths, but independent of soot temperature. It is important to point out, however, that it is necessary to know the morphology of soot aggregates (d_p, k_f, D_f, and N_p distribution) to accurately account for the effect of aggregation on aggregate absorption and emission. In practice, however, this is challenging since the morphology of soot is in general unknown and there are no established, reliable, and in-situ techniques to provide such real-time soot morphology information, though developments in elastic light scattering may lead to a technique for this purpose.

3.2 Effect of aggregation on soot absorption and emission in LII modelling

In this section the effect of aggregation on the soot aggregate laser energy absorption rate was first taken into account in the LII model described by (23) and (24) for the generation of time-resolved aggregate temperature and primary particle diameter of different aggregates sizes from 1 to 850 and a specified initial primary particle diameter of either 30 or 45 nm. The laser wavelength used in the calculations was 532 nm and its temporal profile was the same as that given in our previous studies [11]. The density of soot is assumed temperature independent and has a value of 1.9 g/cm^3. The specific heat of soot was temperature dependent and was given in [33]. Thermal properties associated with soot sublimation, i.e., ΔH_v, M_v, and p_v, were taken from [34]. The effect of aggregation on aggregate conduction heat loss rate was accounted for using the model described in [11], as indicated earlier. The thermal accommodation coefficient of soot was assumed to be constant at 0.37, as in [11]. The initial temperature and the ambient pressure were 1700 K and 1 atm, respectively.

The effect of aggregation on the laser energy absorption of soot aggregates means that aggregates of different size have different temperatures throughout the entire LII process due to the different laser energy absorption rates. In this regard, the present results obtained by solving (23) and (24) are similar to those presented in [14] and will not be shown here. The results calculated under a given aggregate size can be viewed as the true temperature of monodisperse aggregates. Because flame-generated soot often consists of polydisperse aggregates with sizes ranging from 1 to several hundreds or even thousands, 2C-LII experiments in general measure an effective soot temperature based on the incandescence signal ratio. To numerically simulate the 2C-LII experiments, the total incandescence intensities at the two detection wavelengths contributed by an ensemble of polydisperse aggregates can be evaluated using (27), (16), and (17) with the help of the aggregate size dependent temperature and primary particle diameter from solving (23) and (24) as mentioned above.

In the investigation of the aggregation effect on the absorption and emission of soot aggregates in LII modelling, four sets of calculation were conducted for different laser fluences and different initial primary particle diameters. The absorption and emission treatments in the four sets of calculation are summarized in Table 1. A comparison of results between the first and the second treatments highlight the error caused by using the RDG approximation in LII modelling. The third treatment was considered to investigate the error of using the RDG approximation in the calculation of soot emission intensities and emissivity ratio, while the temperatures of individual aggregates were calculated using the GMM model for the aggregate laser energy absorption rate. The fourth treatment was studied because it simulates the current practice of 2C-LII experiments. As such, the signal ratio was provided numerically based on the GMM model for soot laser absorption rate and the LII signal intensities were calculated in place of experimentally measured intensities, but the RDG approximation was employed to provide the soot emissivity ratio.

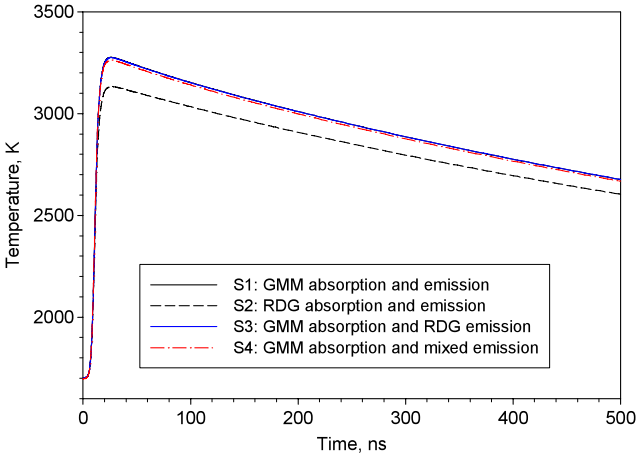

Fig. 7 Effective soot temperatures calculated by different combinations of the GMM and RDG aggregate absorption and emission models for: $F_0 = 0.6$ mJ/mm^2, $d_p = 30$ nm, a lognormal distribution of N_p with $N_g = 40$ and $\sigma_g = 3.5$

Table 1 Four combinations of the soot aggregate absorption and emission treatments in LII modelling

Aggregate absorption and emission description	Aggregate absorption cross section	Emission intensity calculation, (25), (26)	Emissivity ratio calculation, (17)
S1: GMM absorption and emission	GMM	GMM	GMM
S2: RDG	RDG	RDG	RDG
S3: GMM absorption and RDG emission	GMM	RDG	RDG
S4: GMM absorption and mixed emission	GMM	GMM	RDG

The effective temperatures based on the calculated ratio of incandescence intensities at $\lambda_1 = 400$ nm and $\lambda_2 = 780$ nm from the GMM and RDG aggregate absorption and emission models for a lognormally distributed ensemble of aggregates shown in Fig. 5 and an initial primary particle diameter of $d_p = 30$ nm are compared in Fig. 7. These results were obtained for a laser fluence of $F_0 = 0.6$ mJ/mm^2, which is clearly in the low-fluence regime since the peak

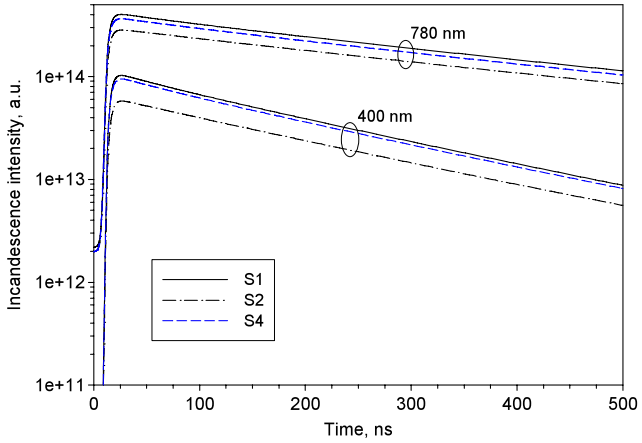

Fig. 8 LII signals calculated by different combinations of the GMM and RDG aggregate absorption and emission models for: $F_0 = 0.6$ mJ/mm^2, $d_p = 30$ nm, a lognormal distribution of N_p with $N_g = 40$ and $\sigma_g = 3.5$

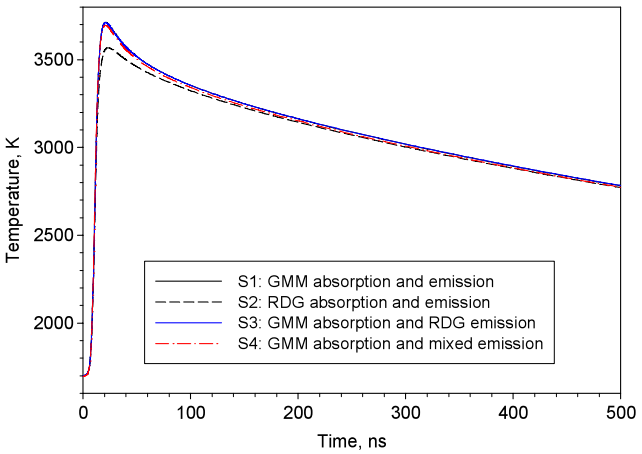

Fig. 9 Effective soot temperatures calculated by different combinations of the GMM and RDG aggregate absorption and emission models for: $F_0 = 0.8$ mJ/mm^2, $d_p = 30$ nm, a lognormal distribution of N_p with $N_g = 40$ and $\sigma_g = 3.5$

effective temperatures are around 3200 K and there is virtually no soot sublimation. The peak effective soot temperature calculated by the RDG model for aggregate absorption and emission (S2) is 143 K lower than that calculated by the GMM model (S1). The difference between the results of the two models remains over a long time, albeit the difference decreases slowly with time due to the slight difference in heat conduction loss rates. Also plotted in Fig. 7 are the results of the third and the fourth sets of calculation summarized in Table 1. The results of using GMM for absorption but RDG for emission (S3) are almost identical to those based on the GMM model for both absorption and emission (S1) and the two curves overlap each other in Fig. 7. These results can be attributed to an error cancellation mechanism. Use of the RDG approximation leads to errors in both the LII intensity ratio and the soot emissivity ratio. These ratios are either both higher or both lower than those from GMM. Therefore, the ratio $\Re/\phi$ does not deviate significantly from that of the GMM model and neither does the effective soot temperature based on (12). It is noticed that the fourth case, S4, has the same signal ratio as that for using GMM for both absorption and emission (S1), but a different aggregate emissivity ratio in the calculation of the effective temperature from the signal ratio. As expected from the results shown in Fig. 6, the results of this case are indeed slightly lower than the results of using GMM for both absorption and emission (S1). The results shown in Fig. 7 highlights that the effect of aggregation on soot aggregate absorption is dominant over its effect on soot aggregate emission in 2C-LII applications, since the absorption cross section is required to calculate the laser energy absorption rate by soot aggregates, but only the ratio of soot emissivities at the two detection wavelengths is needed to infer soot temperature from the signal ratio.

It is also of interest to examine how aggregation affects the LII signals at 400 nm and 780 nm of the lognormally distributed soot aggregates. The LII signals are calculated using (25) and (26) with the aggregate number density set to 1 per unit volume and are shown in Fig. 8. These results are relevant to understanding the effect of aggregation in LII application with detection at a single wavelength. Results of S3 are not shown since they are essentially identical to those of S1. The significantly lower LII signals at the end of the laser pulse (and thereafter) calculated from S2 are due to the lower laser energy absorption rate using the RDG-FA approximation. In addition, the LII signals calculated from the GMM model, S1, exhibit a higher decay rate than those from the RDG-FA approximation, S2. In fact, aggregation also has a similar influence on the decay rate of the effective temperature shown in Fig. 7, i.e, the decay rate of GMM curve (S1) is somewhat higher than that of RDG (S2). This effect of aggregation on either the LII signal decay or the effective temperature decay implies that aggregation will affect the primary particle size derived from the decay rate of either the LII signal or the effective soot temperature.

Effective soot temperatures for a higher laser fluence of $F_0 = 0.8$ mJ/mm^2 and initial primary particle diameter of 30 nm are compared in Fig. 9. The peak temperatures at this fluence are around 3700 K, so there is a small amount of soot sublimation. The peak effective soot temperature calculated by the RDG aggregate absorption and emission model (S2) is 145 K lower than that calculated by the GMM model (S1). The difference between the results of the two models decreases rapidly with time and at 500 ns from the beginning of the laser pulse the difference becomes negligible. This is attributed to the sublimation cooling in the case of using the GMM model, which rapidly lowers the soot temperature near the end of the laser pulse and shortly after. Similar

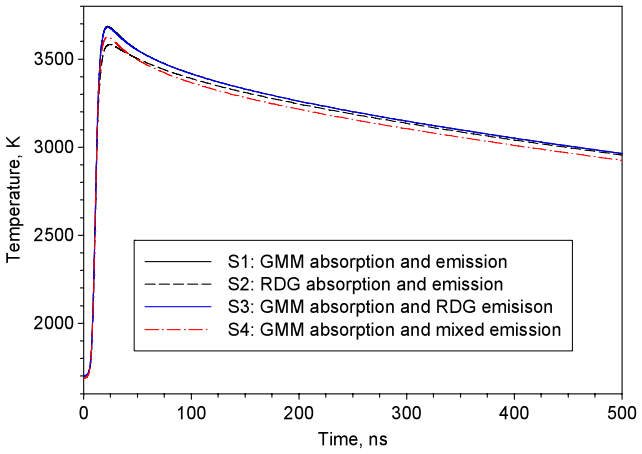

Fig. 10 Effective soot temperatures calculated by different combinations of the GMM and RDG aggregate absorption and emission models for: $F_0 = 0.8$ mJ/mm^2, $d_p = 45$ nm, a lognormal distribution of N_p with $N_g = 40$ and $\sigma_g = 3.5$

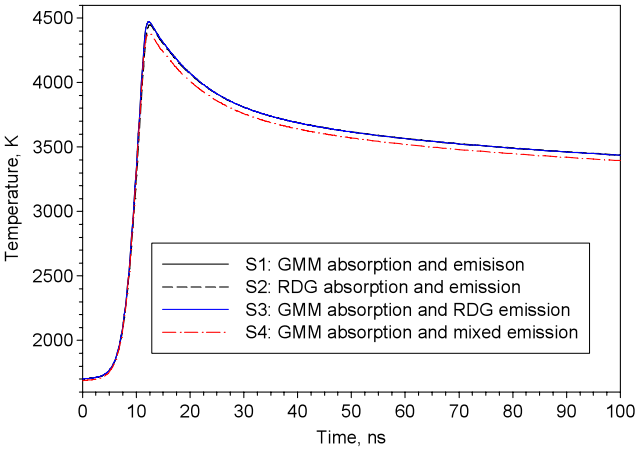

Fig. 11 Effective soot temperatures calculated by different combinations of the GMM and RDG aggregate absorption and emission models for: $F_0 = 2.0$ mJ/mm^2, $d_p = 45$ nm, a lognormal distribution of N_p with $N_g = 40$ and $\sigma_g = 3.5$

observations for the results of S3 and S4 to those in Fig. 7 can be made. The results shown in Fig. 9 once again indicate that it is important to account for the effect of aggregation on soot laser energy absorption, but it is unnecessary to use the GMM model for aggregate emission in LII applications under conditions of typical laminar diffusion flames at atmospheric pressure, where the primary particle diameters are in general less than about 30 nm and the aggregate size distribution is relatively narrow as shown in Fig. 5.

At even higher laser fluences, the effect of aggregation on aggregate absorption diminishes, since the rapid cooling of soot through sublimation in the high laser fluence regime dominates over the relatively small difference in the laser energy absorption rates of different aggregate sizes [14]. This can also be understood by the well-known fact in LII experiments that the fluctuations in the laser pulse energy become less important when the laser fluence reaches the 'plateau' region. The present numerical results of the effective soot temperatures of the lognormally distributed polydisperse aggregates show that the difference in the effective soot temperature between the GMM model (S1) and the RDG model (S2) diminishes as the laser fluence increases. At $F_0 = 1.5$ mJ/mm^2 the difference becomes negligible.

To demonstrate the effect of the initial primary particle diameter on how the GMM and RDG aggregate absorption and emission models affect the calculated effective soot temperature, further numerical calculations were conducted with a larger initial primary particle diameter of $d_p = 45$ nm. All the thermal properties of soot, aggregate size distribution, and the laser properties remain unchanged. For a relatively low fluence of $F_0 = 0.8$ mJ/mm^2 the effective soot temperatures calculated with the four different combinations of the GMM and RDG aggregate absorption and emission models summarized in Table 1 are compared in Fig. 10. The peak temperature predicted by RDG (S2) is 103 K lower than that predicted by GMM (S1). The difference in the effective soot temperatures from RDG and GMM models decreases gradually with time, due to the somewhat higher soot sublimation cooling in the GMM results at this laser fluence. Once again the use of RDG for soot emission only (S3) has negligible influence on the effective temperature as long as GMM is used for soot absorption, which is confirmed by the virtually indistinguishable results for these two cases, as shown in Fig. 10. The only difference between the black solid curve (S1) and the red dash-dot curve (S4) lies in how the emissivity ratio of the lognormally distributed aggregates was calculated. It is noticed that they have the same signal ratio for arriving at the effective temperature, (16). Therefore, these two cases best illustrate the effect of selecting different aggregate emission models in the inferred soot temperature in 2C-LII experiments. Consistent with the results shown in Fig. 6, use of the RDG for the emissivity ratio of polydisperse aggregates leads to a somewhat lower effective temperature (about 60 K) compared to that by using the GMM model for a given signal ratio.

As the last example to illustrate the effect of aggregation on aggregate absorption and emission, calculations were conducted at a significantly higher laser fluence of $F_0 = 2$ mJ/mm^2 and an initial primary particle diameter of $d_p = 45$ nm. The results at this high fluence are compared in Fig. 11. As already mentioned earlier, the difference in soot temperatures predicted by the GMM and RDG aggregate absorption and emission models at high fluences diminishes. This is clearly seen in Fig. 11 between the GMM results (S1, black solid line) and the RDG ones (S2, black short dashed line). The difference in soot temperatures using either the GMM (S1, black solid line) or the RDG model (S3, blue solid line) for emission is again negligible for the reason discussed earlier. When the RDG model is used to only

evaluate the emissivity ratio of the polydisperse aggregates at the two wavelengths (400 and 780 nm), S4, the soot temperatures are consistently lower by about 90 K right after the peak value, again consistent with the results shown in Fig. 6.

4 Conclusions

The effect of primary particle aggregation on soot aggregate absorption efficiency and emissivity was investigated by using the RDG-FA theory and GMM for the purpose of understanding the error caused by using the RDG-FA theory in the determination of soot temperature based on the ratio of incandescence intensities at two different detection wavelengths in two-color LII experiments. The effect of aggregation on soot aggregate absorption and emission was found to be sensitive to both the aggregate size and the primary particle size parameter. Under conditions of typical laminar diffusion flames at atmospheric pressure, where the primary particle diameters are generally less than about 30 nm and the aggregate size distribution is relatively narrow from 1 to several hundreds, use of the RDG-FA theory to evaluate soot aggregate emissivity leads to small error in the soot temperature in two-color LII experiments. However, such error grows rather quickly with increasing the primary particle diameter. These results suggest that it is important to account for the effect of aggregation on aggregate emissivity in the determination of soot temperature in two-color LII experiments conducted in diffusion flames at high pressures due to much larger primary particles and potentially a much wider aggregate distribution associated with enhanced soot loading. It is a challenge to account for the effect of aggregation on soot emissivity, since the detailed morphology of soot is required for this purpose and such information is in general unavailable and difficult to obtain.

Due to the error cancellation mechanism, use of the RDG-FA theory to calculate the ratio of the incandescence intensities and the ratio of aggregate emissivities at the detection wavelengths only causes negligible error in the effective soot temperature in LII modelling. Under conditions considered in this study use of the RDG-FA theory to determine soot temperature based on measured incandescence signal ratio at two wavelengths in the visible in 2C-LII experiments in general underestimates soot temperatures by about 100 K. The relative error in the derived soot volume fraction is dependent only on the selected detection wavelengths and the relative error in the soot aggregate emissivities at the detection wavelengths.

Under conditions of typical laminar diffusion flames at atmospheric pressure, it is important to take into account the effect of aggregation on soot laser energy absorption, but it is relatively unimportant to account for the effect of aggregation on aggregate emission in low laser fluence LII modelling of polydisperse aggregates, where there is no or only a small amount of soot sublimation. At high laser fluences, where there is significant soot sublimation, the effect of aggregation on soot aggregate laser energy absorption diminishes and the difference in the effective soot temperatures of an ensemble of polydisperse aggregates predicted by the GMM model and the RDG-FA theory for aggregate absorption decreases with increasing laser fluence.

It should be emphasized that the findings from this study are subject to the limitations that the primary particles are assumed to be in point touch and aggregation has no impact on the sublimation mechanism. Further studies should be carried out to investigate the effect of primary particle overlap on the optical properties of soot and how aggregation affects sublimation of soot aggregates.

Acknowledgements The authors appreciate financial support for this work from the PERD AFTER Program, Project C23.006, and the PERD Particles and Related Emissions Program, Project C11.008.

References

1. C. Schulz, B.F. Kock, M. Hoffman, H. Michelsen, S. Will, B. Bougie, R. Suntz, G.J. Smallwood, Appl. Phys. B **83**, 333 (2006)
2. D.L. Hofeldt, SAE Technical Paper 930079 (1993)
3. S. Will, S. Schraml, A. Leipertz, Opt. Lett. **20**, 2342 (1995)
4. D.R. Snelling, G.J. Smallwood, F. Liu, Ö.L. Gülder, W.D. Bachalo, Appl. Opt. **44**, 6773 (2005)
5. D.R. Snelling, F. Liu, G.J. Smallwood, Ö.L. Gülder, Combust. Flame **136**, 180 (2004)
6. T. Lehre, B. Jungfleisch, R. Suntz, H. Bockhorn, Appl. Opt. **42**, 2021 (2003)
7. F. Liu, B.J. Stagg, D.R. Snelling, G.J. Smallwood, Int. J. Heat Mass Transf. **49**, 777 (2006)
8. C.M. Megaridis, R.A. Dobbins, Combust. Sci. Technol. **71**, 95 (1990)
9. Ü.Ö. Köylü, G.M. Faeth, Combust. Flame **89**, 140 (1992)
10. A.V. Filippov, M. Zurita, D.E. Rosner, J. Colloid Interface Sci. **229**, 261 (2000)
11. F. Liu, M. Yang, F.A. Hill, D.R. Snelling, G.J. Smallwood, Appl. Phys. B **83**, 383 (2006)
12. F. Liu, G.J. Smallwood, in *AIAA 2008-3917, AIAA 40th Thermophysics Conference*, 23–26 June 2008, Seattle, Washington, USA (2008)
13. K.J. Daun, ASME J. Heat Transf. **132**, 091202 (2010)
14. F. Liu, G.J. Smallwood, J. Quant. Spectrosc. Radiat. Transf. **111**, 302 (2010)
15. W.H. Dalzell, G.C. Williams, H.C. Hottel, Combust. Flame **14**, 161 (1970)
16. Ü.Ö. Köylü, G.M. Faeth, ASME J. Heat Transf. **115**, 409 (1993)
17. T.L. Farias, M.G. Carvalho, Ü.Ö. Köylü, G.M. Faeth, ASME J. Heat Transf. **117**, 152 (1995)
18. F. Liu, K.J. Daun, V. Beyer, G.J. Smallwood, D.A. Greenhalgh, Appl. Phys. B **87**, 179 (2007)
19. C.F. Bohren, D.R. Hoffman, *Absorption and Scattering of Light by Small Particles* (Wiley, New York, 1983), Chap. 4.7
20. Y.A. Levendis, K.R. Estrada, H.C. Hottel, Rev. Sci. Instrum. **63**, 3608 (1992)
21. M. Kerker, *The Scattering of Light*. (Academic Press, New York, 1969), p. 84
22. M.F. Iskander, H.Y. Chen, J.E. Penner, Appl. Opt. **28**, 3083 (1989)

23. G.W. Mulholland, C.F. Bohren, K.A. Fuller, Langmuir **10**, 2533 (1994)
24. B.T. Draine, P.J. Flatau, Opt. Soc. Am. **11**, 1491 (1994)
25. L. Liu, M.I. Mishchenko, W.P. Arnott, J. Quant. Spectrosc. Radiat. Transf. **109**, 2656 (2008)
26. Y.-L. Xu, Appl. Opt. **34**, 4573 (1995)
27. Y.-L. Xu, Appl. Opt. **36**, 9496 (1997)
28. F. Liu, D.R. Snelling, in *AIAA 2008-4362, AIAA 40th Thermophysics Conference*, 23–26 June 2008, Seattle, Washington, USA (2008)
29. F. Liu, G.J. Smallwood, ASME J. Heat Transf. **132**, 023308-1 (2010)
30. F. Liu, D.R. Snelling, K.A. Thomson, G.J. Smallwood, Appl. Phys. B **96**, 623 (2009)
31. K. Tian, K.A. Thomson, F. Liu, D.R. Snelling, G.J. Smallwood, D. Wang, Combust. Flame **144**, 782 (2006)
32. K.A. Thomson, Ö.L. Gülder, E.J. Weckman, R.A. Fraser, G.J. Smallwood, D.R. Snelling, Combust. Flame **140**, 222 (2005)
33. H.A. Michelsen, F. Liu, B.F. Kock, H. Bladh, A. Boiarciuc, M. Charwath, T. Dreier, R. Hadef, M. Hofmann, J. Reimann, S. Will, P.-E. Bengtsson, H. Bockhorn, F. Foucher, K.-P. Geigle, C. Mounaïm-Rousselle, C. Schulz, R. Stirn, B. Tribalet, R. Suntz, Appl. Phys. B **87**, 503 (2007)
34. G.J. Smallwood, D.R. Snelling, F. Liu, Ö.L. Gülder, ASME J. Heat Transf. **123**, 814 (2001)